J. Appl. Comput. Mech., 8(4) (2022) 1141-1153
DOI: 10.22055/JACM.2020.33054.2138

ISSN: 2383-4536
jacm.scu.ac.ir

Shahid Chamran University of Ahvaz

Journal of Applied and Computational Mechanics

Research Paper

Twin Screw Expanders Profile Optimization Using Surrogate-Based Modelling

Hormoz Abolhasani, Mahdi Moghimi, Mahmoud Ebrahimi

Department of Mechanical Engineering, Iran University of Science and Technology (IUST), Narmak, Tehran 16844, Iran

Received March 26 2020; Revised May 01 2020; Accepted for publication July 08 2020.
Corresponding author: M. Moghimi (moghimi@iust.ac.ir)

Abstract. Twin screw machines can be used as an expander to recover the lost power in various processes causing pressure energy loss. Twin screw expanders (TSEs) have caught the attention of many researchers due to low capital, maintenance and operation costs, long lifespan and their application in two-phase fluids. However, substantial efforts required to enhance their performance. This research describes the optimization of the profile of a TSE with 4-6 lobe configuration - using surrogate-based modeling (SBM). To do so, based on the in-house code developed within FORTRAN, a TSE profile is designed and validated against available data. Then, a mathematical model is developed via of experiments (DOE). Next, the effects of four main profile parameters are investigated on the expander performance in the entire design space. Finally, an optimized combination of parameters is offered using a multi-objective genetic algorithm. 3D computational fluid dynamics (CFD) results show that the optimized profile had more than 7% exergy efficiency compared to the base profile.

Keywords: Twin screw expander, Profile optimization, Design of experiments, Surrogate-Based modeling, CFD.

1. Introduction

A twin screw expander (TSE) functions as a positive-displacement machine for recovering the lost exergy induced by gas pressure reduction. TSEs have been addressed over the past years owing to lower manufacturing, maintenance, and operation costs [1], high reliability in two-phase flow applications [2], and slower rotational speed and, in turn, longer lifespan. However, the performance of twin screw expanders still needs to be improved.

The first notion of utilizing screw machines dates back to 1952. Many researchers have attempted since the early 1970s to generate two-phase expansion turbines. As a method to recover energy loss, studies were performed in 1973 on the use of a screw expander turbine for expanding the pressurized water-steam mixture. In the 1970s, the TSEs were increasingly employed to expand two-phase fluids due to the oil crisis occurrence. In 1976, using empirical correlations, tremendous efforts were put into modeling the expansion process in screw turbines. Sangfors [3] modeled the expansion procedure in these types of machines with quite simple techniques. Steidel et al. [4] studied screw expander on water-steam mixture experimentally for the first time. The study on two-phase expansion was started by Smith [5] depending on the application of screw turbines to produce the driving force. Moreover, such expanders, for expanding high-pressure water, have been found unsuitable [6]. Smith et al. [7] designed and built a laboratory screw expander sample, which was tested with R-113. Satisfactory performance was offered by the screw expander, and the adiabatic efficiency increased to 76%. Stosic et al. [8] and Smith et al. [9] performed a thermodynamic analysis of such machinery using a one-dimensional thermodynamic model. They showed that the expansion efficiency of screw machines depends on various parameters, including the size and shape of the high-pressure port, leakage flows, and the machine's built-in volume ratio. Brummer and Hutker [10] and Hutker and Brummer [11] evaluated the screw expander performance by evaluating length to diameter, volume ratio and rotors wrap angle. The examination of screw expander performance started in 2013 by performing 3D CFD analysis. The clearance effect on the internal leakage was evaluated by Kovacevic and Rane [12] for air (as the working fluid), along with perfectly designing high-pressure port via CFD. They indicated leakage flows significantly impact the efficiency of screw expanders. Papes et al.[13] assessed the effect of the clearance gaps on the expander performance using CFD and R245fa as the working fluid and, in another paper, presented a multi-chamber mathematical model of a TSE to predict its performance [14]. Andres [15], simulated internal leakage flows via 3D CFD, and revealed that they have the most profound impact on the efficiency at high inlet pressures and low speeds.

Recently, the TSE simulations have been based on the CFD technique. However, this tool is unable to analyze the whole design space owing to cost and time restrictions. TSE analysis entails doing a lot of computations; thus, it takes a long time to assess the system behavior in various conditions for a diverse range of parameters. Accordingly, system optimization through CFD efforts is not almost practical. Thus, to comprehensively study TSE, a new tool needs to be added to cover the entire computational space for the design process and optimization at the lowest cost and shortest time feasible. In recent years, several methods have been introduced for this purpose [16–38], one of which is the SBM method.

Published online: February 30 2021

So far, several studies have been carried out on turbomachinery by implementing the SBM method. Forrester and Keane [39], in addition to the investigation of the models applied to SBM, proposed different sample selection approaches and enhanced the available models as well. They recognized the Kriging model as a robust method that can provide highly accurate numerical simulations. Zhu et al. [40] performed blade optimization of a horizontal axis turbine via SBM. They varied four geometric parameters to calculate various pitch angle distributions and, finally, optimized axial propulsion and power coefficient. The Box-Behnken method was implemented to select samples, and quadratic polynomials equations were used for modeling. They implemented optimized multi objective genetic algorithms after modeling to determine the optimal values. Also, they illustrated that the polynomial model could preserve the accuracy of modeling due to fewer design parameters. Bellary et al. [41] made an investigation into the SBM methods by addressing two modeling methods used in optimization problems, namely quadratic polynomial and Kriging. Also, they conducted a sensitivity analysis of turbomachinery and evaluated the accuracy of both methods to optimize a radial blade in terms of efficiency and head. Finally, the optimization results revealed that the use of the Kriging method would yield more accurate results. In ref. [42], they made a comparison among the different Kriging and quadratic polynomials methods coupled with CFD applied to turbomachinery problems. They showed that the Kriging method offered the most accurate predictions, whereas the weakest predictions were provided by the quadratic polynomials. In an optimization problem of a jet engine blade, Tosin et al. [43] implemented the Kriging method to lower the computational costs. Based on the comparison of the results provided by the two optimization methods, namely the evolutionary and gradient-based approaches on the modeling response surface by the Kriging method, they concluded that the gradient based optimization method would yield the superior solution at a higher pace. The effects of flow and geometric parameters on the turbine performance were investigated by Gaiser et al. [44], indicating that SBM could be practical for both experimental and numerical problems. Also, the combination of SBMs has seemed substantially interesting to make more precise predictions. In this respect, a study on the optimization process of a conventional oceanic turbine was carried out by Badhurshah and Samad [45], showing that computation time remained almost unchanged in practice among the use of single or several SBMs.

Optimizing the rotor profile of a TSE is a crucial factor in reducing internal leakage and thus increasing machine efficiency. Since the SBM modeling has not been taken into account in previous studies on the TSE profile, the present study aims at optimizing the profile of a twin-screw expander with 4-6 lobes to reduce the internal leakages using the SBM method and genetic optimization technique. The TSE profile is first designed and validated using a FORTRAN code to develop the SBM. Then, the concerned parameters are selected in a rational range, and preferred samples are chosen out of the design space using the DOE method. Next, the SBM model is developed according to the Kriging function, and the profile is ultimately optimized. Also, a multi-objective genetic algorithm and 3D CFD molding were used to obtain exergy efficiency. The strategy flowchart is shown in Fig. 1.

The general schematic of the profile optimization method is shown in Fig. 2. The results of this new methodology can provide a solid support for the design and optimization of the twin screw machines.

2. TSE Profile Design

The general design method of a TSE rotor profile comprises the application of a primary curve to one rotor and conjugate motion to generate the relevant curve over the other rotor. Thus, a curve is allocated to one rotor at first, and the conjugate profile then forms on the other rotor based on the envelope theory.

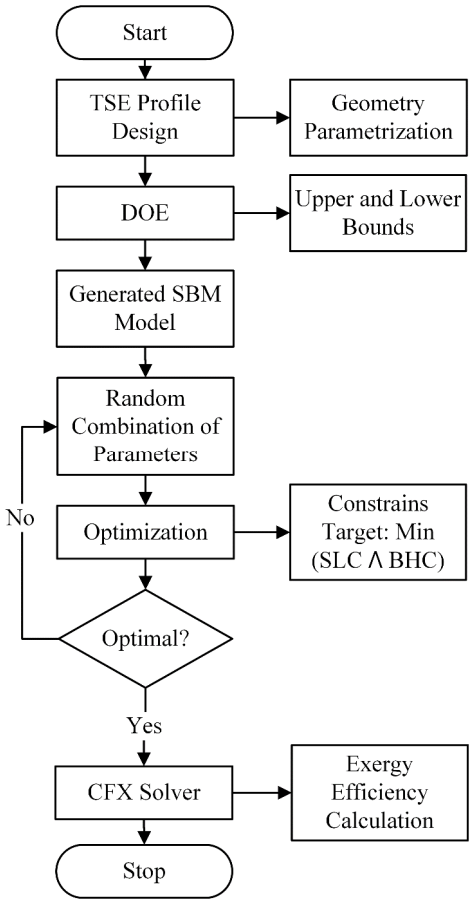

Fig. 1. Study Strategy Description

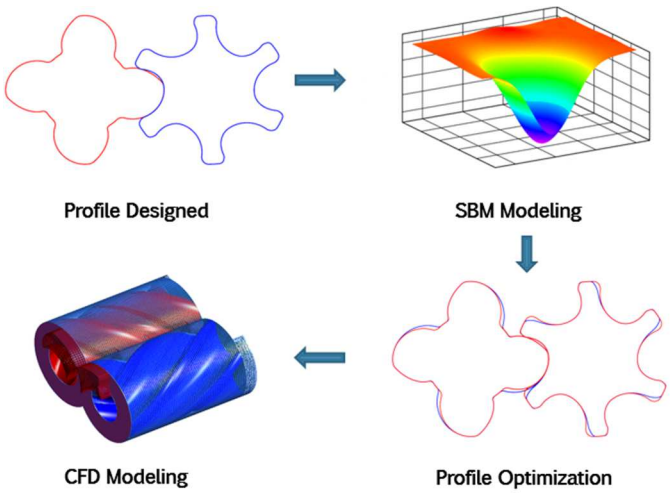

Fig. 2. General schematic of the profile optimization

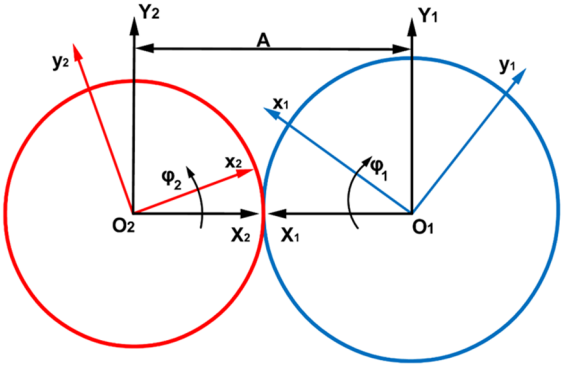

Fig. 3. Rotors coordinate systems

Two coordinate systems are placed on female and male rotors. In Fig. 3, $O_1X_1Y_1$ and $O_2X_2Y_2$ stand for the fixed coordinate systems with origins O_1 and O_2, respectively, coinciding with the centers of male and female rotors. $O_1x_1y_1$ and $O_2x_2y_2$ denote the rotating coordinate systems. On the onset of the movement, $O_1X_1Y_1$ and $O_2X_2Y_2$ coincide with $O_1x_1y_1$ and $O_2x_2y_2$, respectively. Following a short time, the female and male coordinate systems ($O_1x_1y_1$ and $O_2x_2y_2$) rotate clock-wisely and counter clock-wisely around the origins O_1 and O_2 with the angles of φ_1 and φ_2, respectively.

The rotation angle can be described according to the unchanged angular velocity ratio between the rotors, as given by Eq. (1).

$$i = \frac{\varphi_2}{\varphi_1} \tag{1}$$

Let $k = i + 1$, the two rotating coordinate systems are related as follows [46]:

$$\begin{cases} x_2 = -x_1 \cos k\varphi_1 - y_1 \sin k\varphi_1 + A \cos i\varphi_1 \\ y_2 = -x_1 \sin k\varphi_1 + y_1 \cos k\varphi_1 + A \sin i\varphi_1 \end{cases} \tag{2}$$

The female rotor profile's locus, which comprises a set of curves, is obtained in the O1X1Y1 coordinate by Eq. (3),

$$\begin{cases} x_1 = x_1(t, \varphi_1) \\ y_1 = y_1(t, \varphi_1) \end{cases} \tag{3}$$

where t represents the female rotor's curvature parameter. These families of curves generate envelopes for various angles, as the male rotor curve's conjugate. A contact point exists between the generated envelope and each curve, wherein the slope of the curve's tangent is identical and can be written in a point of the envelope as follows [46]:

$$\begin{vmatrix} \frac{\partial x_1}{\partial t} & \frac{\partial x_1}{\partial \varphi_1} \\ \frac{\partial y_1}{\partial t} & \frac{\partial y_1}{\partial \varphi_1} \end{vmatrix} = 0 \tag{4}$$

The above determinant was assumed to represent the envelope condition (i.e., interference equation). The male rotor's conjugate profile can be specified by solving φ_1 (interference equation) and replacing it in Eq. (2). Each profile of the rotor consisted of eight curved sections with different geometric shapes, including circles, cycloids, and epicycloids, which are described on each rotor by a certain number of parameters. These parameters include the center coordinates, the starting and ending angles, the radius, and other geometric parameters. Using envelope theory and applying an in-house code developed in FORTRAN, the segments of the TSE profile were generated (refer to Fig. 4).

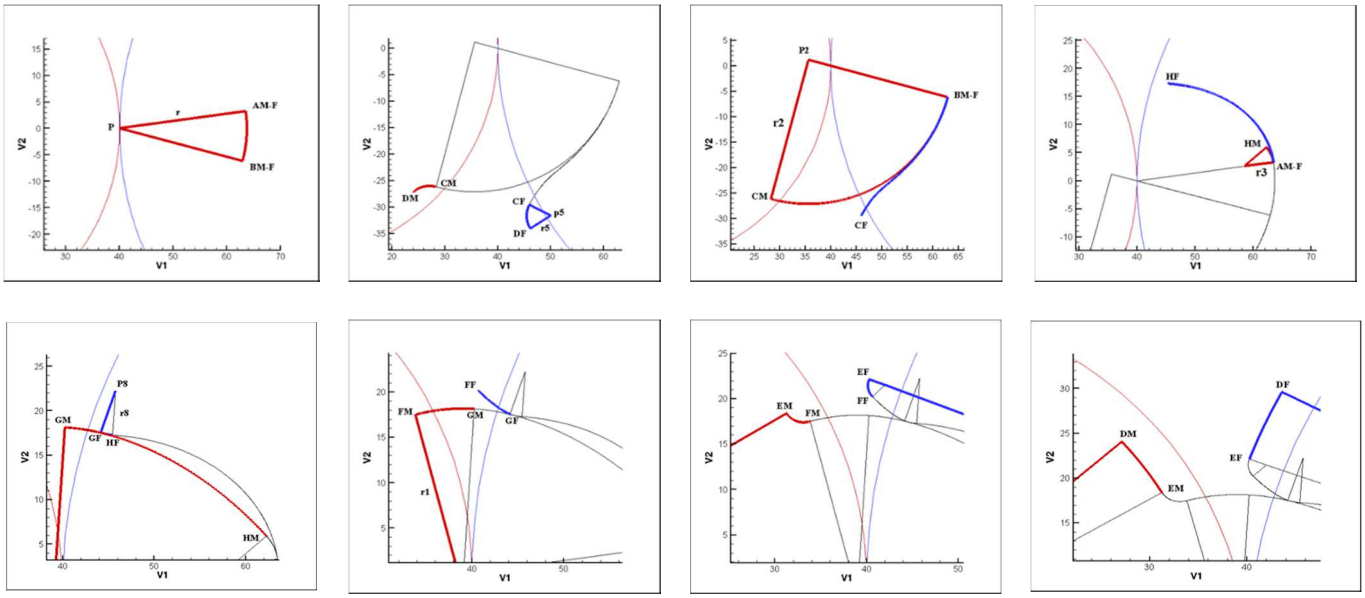

Fig. 4. TSE profile curves

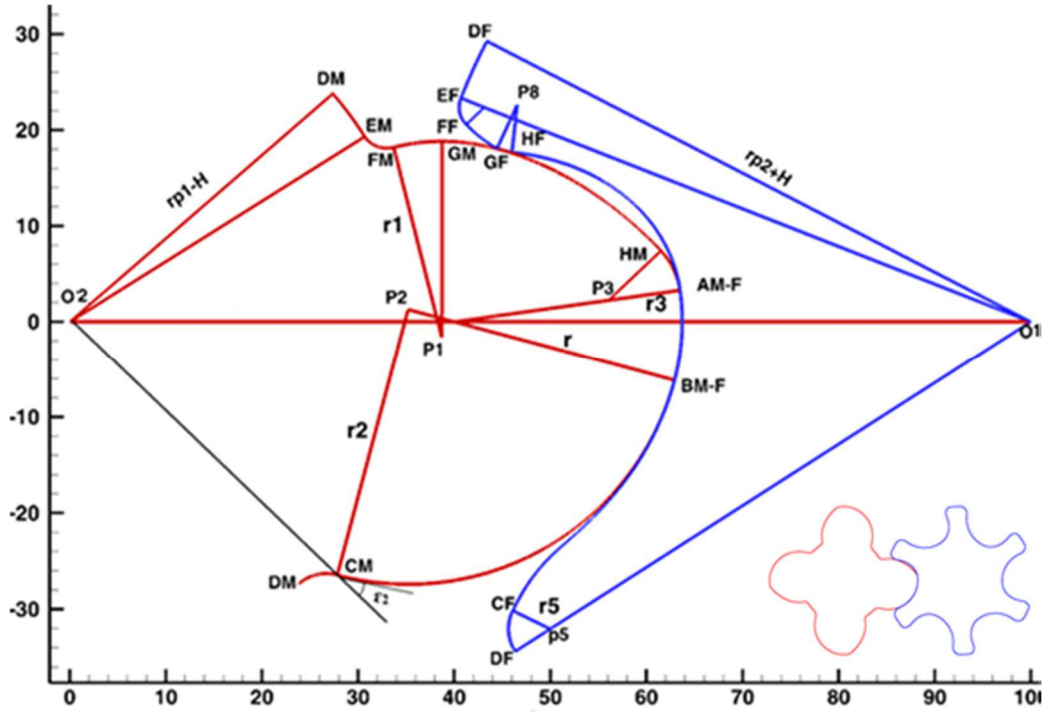

Fig. 5. TSE Generated profile

The expander rotor was obtained by combining the generated segments. TSE 4-6 lobe configuration of the rotor is depicted in Fig. 5.

2.1 Profile validation

After designing the profile, the results were validated against the available data [46], as presented in Table 1.

The results indicated that the designed profile was consistent with the base profile in a reasonable manner and, accordingly, the code-based design was produced correctly. Four parameters of the profile were studied to reduce internal leakage and increase machine efficiency as a result.

3. Design of Experiment

The functionality of any design depends on several parameters whose changes affect the output and performance of a system. In complex problems, it takes a long time to find the optimum design, which is problematic and costly. Thus, the DOE is vital to minimize the required iterations to determine the optimal design parameters. According to the literature and Table 2, four profile parameters were chosen in this study as effective factors. The parameters effects were discretely investigated on the expander performance.

Table 1. Designed profile comparing to available data

Female profile				
Points	Designed profile		Available data [46]	
	x (O_1=0.0)	Y	x	y
DF	**77023.53**	**-19997.34**	**7702.53**	**-2000.34**
CF	1574.54	-35299.30	157.54	**-3530.30**
BF	8341.37	-14048.6	834.37	**-1405.6**
AF	50589.36	30188.3	5059.36	**3019.3**
HF	99695.53	68107.17	9969.53	**6811.17**
GF	55.59233	18.12565	5920.55	**1258.18**
FF	58.79112	20.58657	7901.58	**5867.2**
EF	59.33257	23.24886	3326.59	**2489.23**
Male profile				
Points	Designed profile		Available data [46]	
	x (O_2=0.0)	y	x	y
DM	94778.23	-27.24664	23.9478	-27.2466
CM	64822.27	-26.39191	27.6482	-26.3919
BM	91659.62	-6.14048	62.9166	-6.1405
AM	49412.63	3.30188	63.4941	3.3019
HM	49719.61	7.43148	61.4972	7.4315
GM	38.40914	18.81338	38.4090	18.8135
FM	33.71387	18.16683	33.7140	18.1673
EM	30.73111	19.27394	30.7307	19.2743

Table 2. Quantification of parameters

Parameters		Description	Unit	Lower bound	Upper bound
Factors	P1(β2)	End angle of the arc AM-BM	Degree	13	20
	P2(tg)	End angle of the arc HM-GM	Degree	110.5	114.3
	P3(tf)	End angle of the arc GM-FM	Degree	102.7	106.5
	P4(ε2)	Pressure angle	Degree	23	34
Response	P5(SLC)	Sealing line constant	dimensionless	Response surface	
	P6(BHC)	Blow-Hole constant	dimensionless	Response surface	

Table 3. Sample selection based on the LHS

Design points	P1	P2	P3	P4
1	16.5	113.92	102.928	27.62
2	19.58	113.768	104.296	28.94
3	16.22	111.032	105.268	25.86
4	16.78	114.224	105.056	26.3
5	13.98	112.096	103.992	32.9
6	17.06	112.4	102.776	32.02
7	18.18	113.616	106.272	30.7
8	19.3	111.488	104.904	24.98
9	19.86	111.792	103.84	31.14
10	15.38	112.704	106.124	28.5
11	14.26	112.248	103.384	23.66
12	17.9	113.312	104.448	33.78
13	17.62	111.336	103.232	26.74
14	19.02	111.64	105.6	30.26
15	15.1	114.072	104.752	32.46
16	13.14	113.464	105.36	27.18
17	18.46	112.856	103.536	24.1
18	18.74	113.008	105.816	24.54
19	14.54	110.728	104.144	25.42
20	13.7	113.16	103.688	28.06
21	13.42	111.184	105.312	29.38
22	15.66	112.552	105.208	23.22
23	15.94	111.944	105.664	33.34
24	14.82	110.88	103.08	29.82
25	17.34	110.576	104.6	31.58

These parameters created a 4D design space wherein an optimal point of profile performance should be detected. Moreover, the parameters interactions and effects were desirable on the internal leakage of the expander. Also, the supreme design point was sought in the study scope. One of the most viable methods for sample selection is Latin Hypercube Sampling (LHS), wherein the samples are selected so that the design parameters' values were allocated to all samples only one time. The LHS method's flexibility provides the most trustworthy sample selection in the DOE approach [47]. The LHS-based sample selection results are listed in Table 3.

Blow hole constant (BHC) and sealing line constant (SLC) were computed for each sample. The minimization of these two parameters had a key role in reducing internal leakage and increasing expander efficiency.

The blow hole is defined as a small triangular-shaped area, which is formed by the female and male rotor tips and the housing cusp. The BHC is the dimensionless ratio that can be written as:

$$BHC = \frac{A_b * \tan\beta_{pitch}}{(A_1 + A_2) * \sin\beta_{ftip}} \tag{5}$$

where A_b is the Blow hole area, β_{pitch} indicates screw angle on the pitch circle, β_{ftip} represents screw angle at the tip of female rotor and A_1 & A_2 equal to the cross-sectional area bounded by male and female rotor profile and the housing bore.

The SLC is the dimensionless ratio that can be indicated as:

$$SLC = \frac{L_s}{A} \tag{6}$$

where L_s is the length of the sealing line between the female and male rotors, and A is equal to the distance between the center of the rotors. The calculation results for BHC and SLC for each of the samples are shown in Fig. 6.

BHC and SLC calculations were time-consuming for any of the parameter combinations; therefore, it was not possible to study all of the design space in a short time. As a result, there was a need for an alternative model to study the design space in the least possible time.

4. SBM

The SBM is used to reach a function for calculating the BHC and SLC within the whole design space. The approximation of a continuous space is needed by combining several functions to construct this model. As indicated in Table 3, the set of selected samples are denoted by $\vec{X} = \{\vec{x}^{(1)}, \vec{x}^{(2)}, \ldots, \vec{x}^{(n)}\}^T$, and the problem output is then represented by $\vec{Y} = \{\vec{y}^{(1)}, \vec{y}^{(2)}, \ldots, \vec{y}^{(3)}\}^T$. Later, the approximate function (f) should be found [48], as calculated by Eq. (7).

$$\hat{f}(x^j) = \sum_{i=1}^{n_c} w_i \psi(\|x^j - c^i\|) = y^j \tag{7}$$

where ψ stands for a radial-basis function playing a critical role in the SBM model output provided that it is correctly selected [49]. Estimating modeling parameters crucially depends on the weight calculation by $\vec{w} = \Psi\vec{y}$. Here, Ψ represents the Gram matrix that is defined as:

$$\Psi = \psi(\|x^{(i)} - x^{(j)}\|) \tag{8}$$

Besides, the selection of the radial-basis function is important. For instance, Gaussian function ($\psi(r) = e^{-r^2/(2\sigma^2)}$) usage in specific conditions leads the Gram matrix to be symmetric, which lowers the costs of computations. The Kriging function is broadly utilized in the defined SBM modeling as a radial-basis function, as written below:

$$\psi^{(i)} = exp\left(-\sum_{j=1}^{k} \theta_j \left|x_j^{(i)} - x_j\right|^{p_j}\right) \tag{9}$$

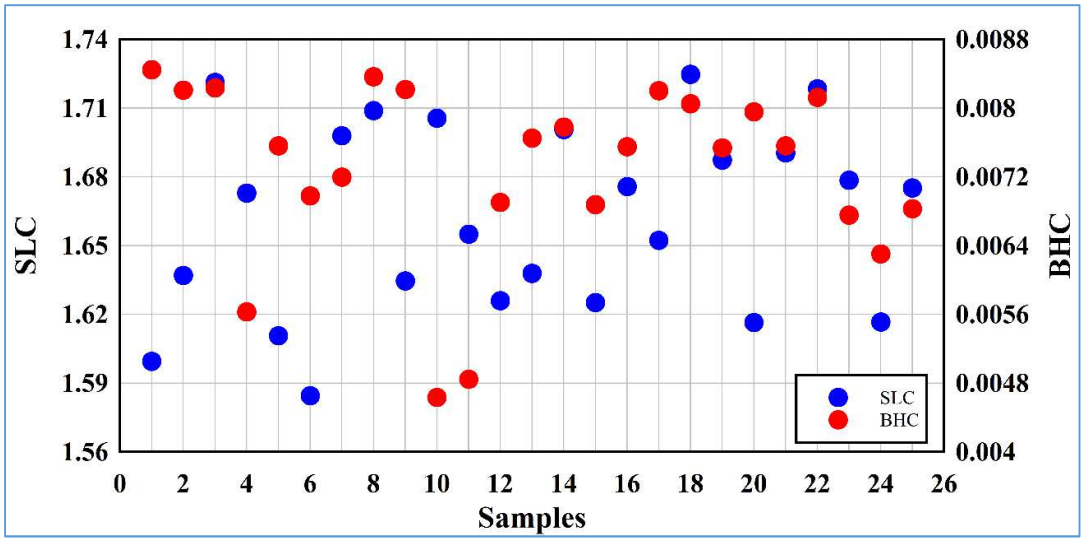

Fig. 6. Contact line and blow- hole area constant of samples

This function is identical to the Gaussian function, aside from the fact that the equation is multiplied by $\theta_j = \{\theta_1, \theta_2, \dots, \theta_k\}^T$ in the Kriging method rather than a constant value (e.g., 1/σ2), permitting the basis function width to have a variable-to-variable shift. Also, the exponent is set at 2.0 in the Gaussian basis-radial function, generating a smooth function in point $x^{(i)}$. In the Kriging function, this exponent ($p_j = \{p_1, p_2, \dots, p_k\}^T$) is allowed to change (typically $p_j \in [1,2]$) for all dimensions in x [50], which provides a more precise approximation. Typically, the SBM model is based on the Kriging function to calculate BHC, assuming ε2 and β2 to be constant (shown in Fig. 7). For the base profile, the BHC and SLC are 7.107 x 10^{-3} and 1.6117, respectively [40]. The corresponding values predicted by the SBM were 7.1065 x 10^{-3} and 1.6118, respectively; therefore, the BHC and SLC were well estimated with the SBM.

5. Optimization

Given the development of the SBM and prediction of the output in the whole design space, optimum points can be sought by a multi objective genetic algorithm which assumes SLC and BHC as target functions (both of them need to be minimized) with the information listed in Table 2 (as the preferred constraints) based on the following flowchart (see Fig. 8).

The optimization was initiated by generating studied chromosomes (β_2,t_g,t_f,ε_2) randomly in the design space (Fig. 9), called the initial population. All the generated chromosomes were decoded, and SLC and BHC were calculated. Then, genetic selection operators were employed to select superior chromosomes, and the mutation and crossover operators were used to produce new chromosomes. Also, the next-generation's population was chosen, while chromosomes were gradually directed towards the optimized points within a gradually developmental process [51]. Each generation included a population of 200 to obtain the optimal point, and the algorithm pursued 30 generations.

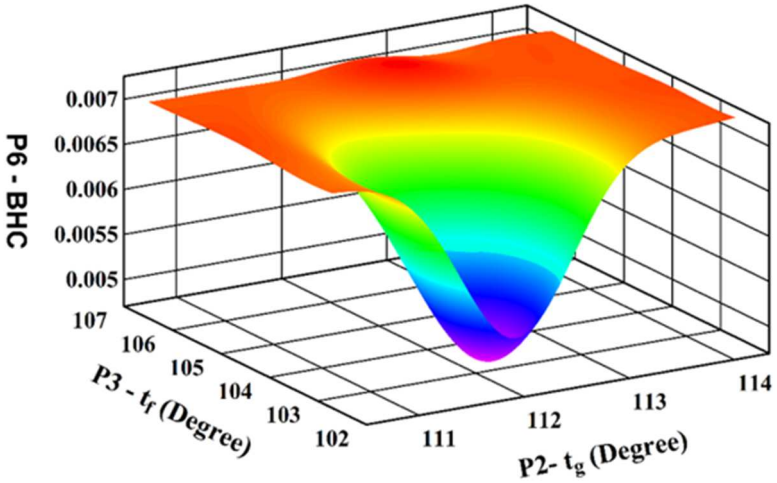

Fig. 7. BHC surrogate-based modeling

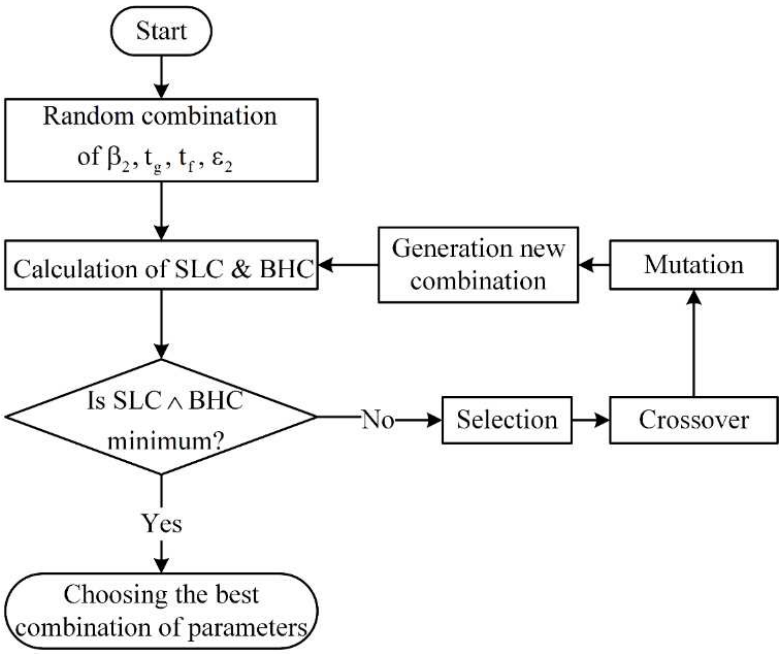

Fig. 8. Optimization flowchart

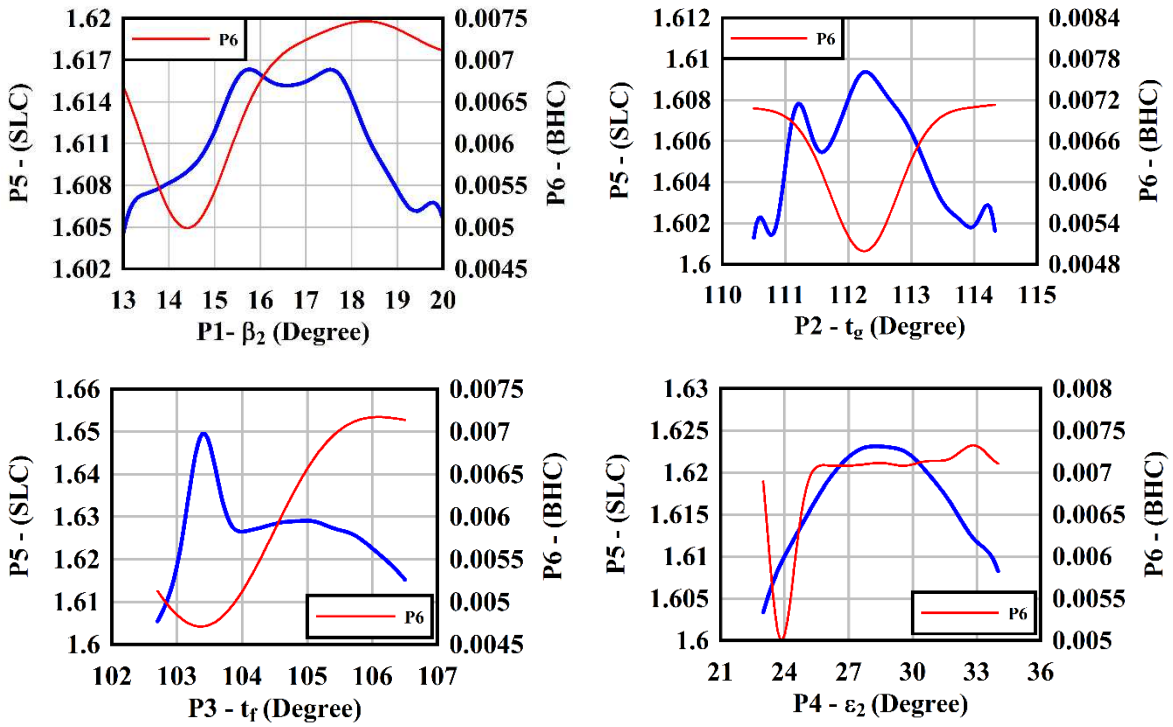

Fig. 9. Studied parameters Vs. BHC and SLC

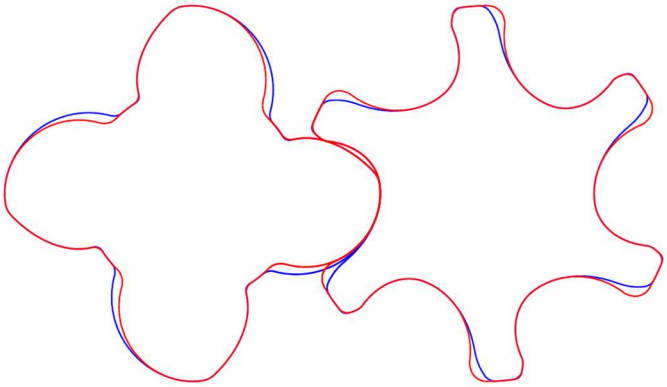

Fig. 10. Optimized profile (Blue) relative to the base profile (Red)

For the optimized profile shown in Fig. 10, the BHC and SLC were 4.9905 x 10^{-3} and 1.609, respectively. BHC was reduced by 29.8% compared to the base profile, showing the significant enhancement of profile performance.

In this phase, the exergy efficiency of each profile was computed using 3D CFD modeling based on the TSE technical specifications in Table 4.

Table 4. TSE Technical Specifications

Parameter	Value	Unit
Female lobes (Z1)	6	-
Male lobes (Z2)	4	-
Center of rotors (A)	100	mm
Wrap angle (ψ)	300	Degree
Diameter of mail rotor (D)	127.45	mm
Length to Diameter (L/D)	1.406	-
Volume ratio (Vi)	1.47	-

6. CFD Modeling

In the CFD modeling, the Navier-Stokes differential equations are converted to algebraic equations by discretizing the solution domain into computational cells. Also, a set of linear equations is generated by applying boundary conditions. An approximate solution was obtained almost accurately by solving these equation sets for all elements and several iterations. A CFD model was used to simulate the 3D fluid flow in the TSE. A reliable numerical solution needs to be obtained as the prerequisite of the simulation model, which entails designing geometry, boundary conditions, meshing, and solving procedure.

6.1 Geometry and meshing

The geometry of the TSE model was divided into five major parts, including inlet port, male rotor, casing, female rotor, and the outlet port (Fig. 11).

An in-house code based on algebraic approach [52] was written for the generation of structured (hexahedral) moving mesh between two rotors. However, an unstructured (tetrahedral) grid was produced for outlet and inlet ports using ANSYS ICEM 16.2. The solver was first provided with numerical grids (by the code) at all time steps, followed by updating the meshes for various rotor positions via an external subroutine.

6.2 Boundary conditions

ANSYS CFX was utilized to provide a 3D modeling of TSE and the Spallart-Almaras method was implemented to model flow turbulence. Dry air (as an ideal gas with a dynamic viscosity of 1.831x10-5 kg/ms, specific heat capacity of 1004.4 J/kg.K, molar mass of 28.96 kg/kmol, and thermal conductivity of 2.61x10-2 W/m.K) entered the expander at the pressure of 2.0 bar and temperature of 350 K with the opening boundary condition. It left the expander at the pressure of 1.0 bar and temperature of 298 K after expansion. The mesh dependency on the expander output power is shown in Fig. 12 for the filling pressure of 2.0 bar and rotational speed of 4000 rpm. As depicted, the minimum required quantity of cells is about 1055345.

The pressure expansion curve was depicted in Fig. 13. As can be observed, the inlet port was opened at first, and high-pressure air entered the expander. Later, the inlet port was closed at point A, and the expansion process continued to point B where the outlet port was opened to initiate the discharge process.

7. Exergy Analysis

The sink-and-source method was applied to determine expander exergy efficiency. The gas flow and net axial work were expressed as the exergy source and sink, respectively. The torque exerted on each rotor at the rotational speed of 4000 rpm and filling pressure of 2.0 bar is illustrated in Fig. 14.

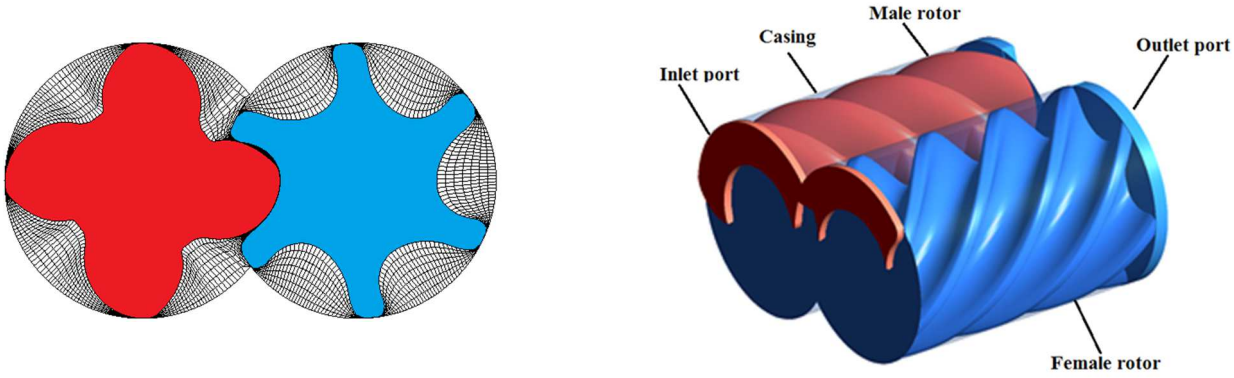

Fig. 11. TSE simulation model

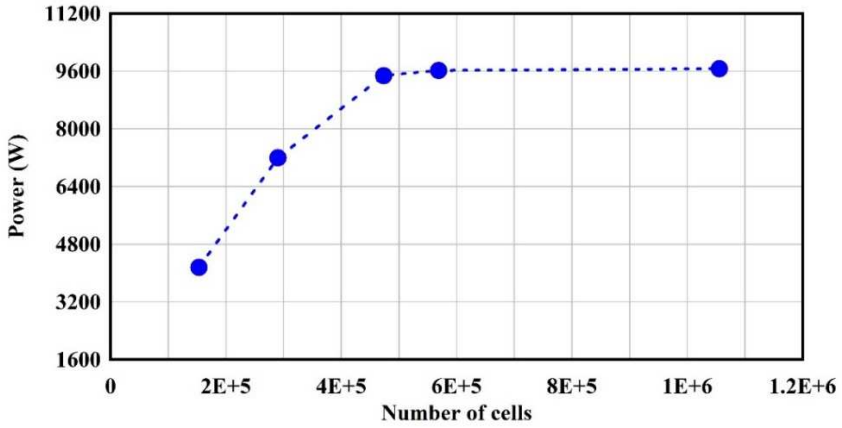

Fig. 12. Mesh dependency of the power

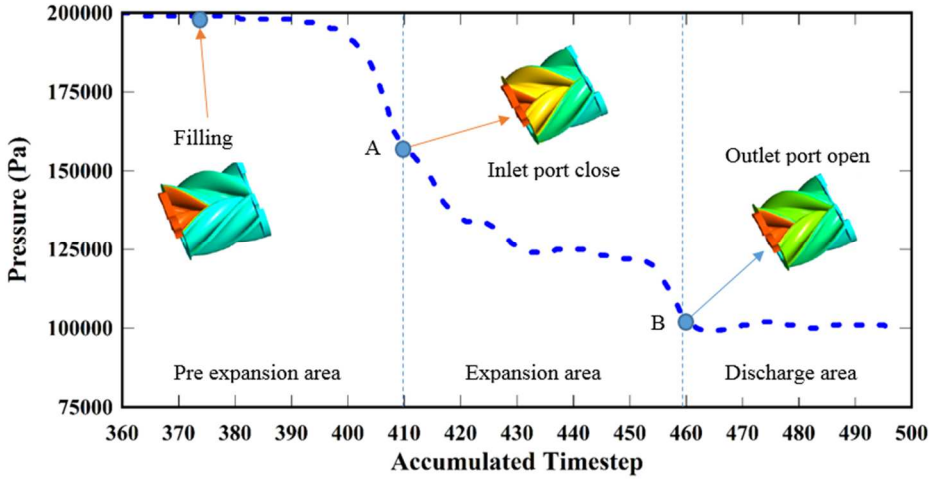

Fig. 13. TSE expansion curve

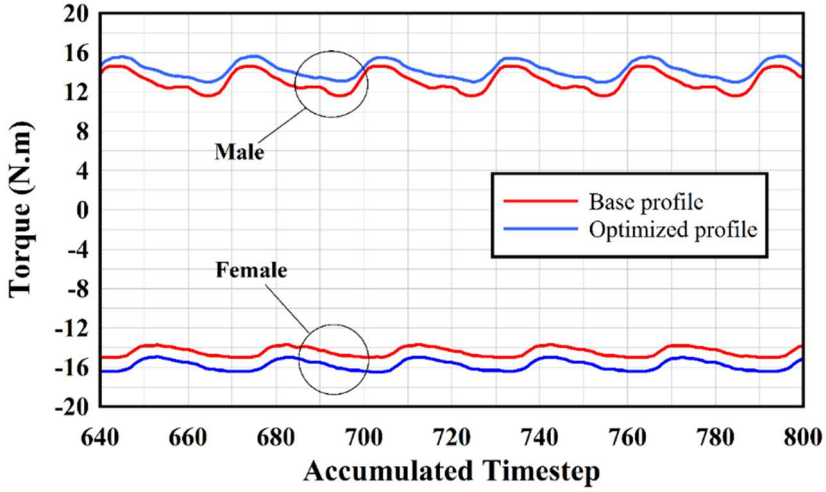

Fig. 14. The torque applied on the male and female profile

The power generated by the TSE was calculated as the exergy sink based on the mean torque exerted on the rotors for one complete rotation (male rotation of 360 degrees), i.e., four expansion cycles.

$$\Delta EX_{sink} = \frac{2\pi n.(\tau_{\text{male}} + (\frac{Z_2}{Z_1}).\tau_{\text{female}})}{60} \tag{10}$$

The available exergy is defined as:

$$\Delta EX_{source} = n \cdot R \cdot \mathrm{T}_0 \cdot Ln\left(\frac{P_1}{P_2}\right) + \dot{m}.(h_1 - h_2)\left(1 - \left(\frac{\mathrm{T}_0}{\mathrm{T}_1 - \mathrm{T}_2}\right) Ln\left(\frac{\mathrm{T}_1}{\mathrm{T}_2}\right)\right) \tag{11}$$

and, the exergy efficiency is written as:

$$\eta_{ex} = \frac{\Delta EX_{sink}}{\Delta EX_{source}} \tag{12}$$

As to a combination of studied parameters (in agreement with the experimental model) the exergy efficiency determined by the SBM via the Kriging method was consistent with that provided by CFD simulations (Table 5).

The optimization results showed the superiority of the SBM approach to designing an accurate profile.

Table 5. Comparison between geometrically optimized and the available turbine

Description	BHC	SLC	Exergy efficiency
Base Profile	0.0071070	1.6117	81.10 %
Optimized Profile	0.0049905	1.6090	88.40 %

8. Conclusion

In this study, twin screw expander was considered as an effective tool for recovering exergy. Optimization of the TSE profile was performed by combining DOE and SBM to analyze the design space and improve the exergy efficiency. To construct the SBM model, the samples' matrix were first formed by LHS approach using the combination of four geometric parameters as input variables. Next, the BHC and SLC of the TSE profile were calculated for each combination. Then, according to the results, an alternative model was obtained, called SBM. Subsequently, using a multi-objective genetic algorithm aiming to minimize BHC and SLC, the well-suited combination of parameters was extracted. Based on the CFD modelling, the optimized profile had more than 7% exergy efficiency compared to the base profile. The results revealed that SBM modeling throughout the design space would yield a more efficient TSE profile in the shortest time.

Author Contributions

The manuscript was written through the contribution of all authors. All authors discussed the results, reviewed, and approved the final version of the manuscript.

Acknowledgments

Not applicable.

Conflict of Interest

The authors declared no potential conflicts of interest with respect to the research, authorship, and publication of this article.

Funding

The authors received no financial support for the research, authorship, and publication of this article.

Data Availability Statements

The datasets generated and/or analyzed during the current study are available from the corresponding author on reasonable request.

Nomenclature

A	Rotors Center distance (mm)	t_c	End angle of the arc BM-CM (Degree)
D	Diameter of Mail rotor (mm)	t_f	End angle of the arc GM-FM (Degree)
h	Enthalpy (kJ/kg)	t_g	End angle of the arc HM-GM (Degree)
L	length of rotors (mm)	t_h	End angle of the arc AM-HM (Degree)
$\dot{m}$	Mass flow rate (kg/s)	Z	Rotor number of lobes
n	Rotational speed (rpm)	φ	Rotational angle (Degree)
P	pressure (bar)	$\boldsymbol{\psi}$	Main rotor wrap angle (Degree)
r_f	Gate Pitch circle radius (mm)	β2	End angle of the arc AM-BM (Degree)
r_m	Main Pitch circle radius (mm)	ε2	Pressure angle (Degree)
T	Temperature (K)	CFD	Computational fluid dynamics
τ	Torque (N.m)	SBM	Surrogate based modeling
t	Time (second)	TSE	Twin screw expander

References

[1] Smith, I. K., Stosic, N., and Kovacevic, A., Screw expanders increase output and decrease the cost of geothermal binary power plant systems, *Transactions - Geothermal Resources Council*, 29 October, 2005, 787–794.
[2] Brummer, A., Influence of liquid in clearances on the operational behavior of twin screw expanders, *9th International Conference on Compressors and their Systems*, 12060, 2015.
[3] Sangfors, B., Analytical Modeling of Helical Screw Machine for Analysis and Performance Prediction, *Compressor Technology Conference*, Purdue, 482–487, 1982.
[4] Steidel, R. F., Pankow, D. H., Brown, K. A., The empirical modelling of a Lysholm screw expander, *Proc. 18th Intersociety Energy Conversion Engng. Conf. on Energy for the Marketplace*, Florida, 286–293, 1983.
[5] Smith, I. K., Development of the Trilateral Flash Cycle System: Part 1: Fundamental Considerations, *Proceedings of the Institution of Mechanical Engineers, Part A: Journal of Power and Energy*, 207, 1993, 179–194.
[6] Smith, I. K., Stosic, N., and Aldis, C. A., Development of the Trilateral Flash Cycle System: Part 3: The Design of High-Efficiency Two-Phase Screw Expanders, *Proceedings of the Institution of Mechanical Engineers Part A: Journal of Power and Energy*, 210(1), 1996, 75–93.
[7] Smith, I. K., Stosic, N., Aldis, C. A., Kovacevic A., Twin Screw Two - Phase Expanders in Large Chiller Units, *Imeche Conference Transactions*, 105–114, 1999.
[8] Stosic, N., Smith, I. K., Kovacevic,A., A Twin Screw Combined Compressor And Expander For CO2 Refrigeration Systems, *International Compressor Engineering Conference*, London, 1-9, 2002.
[9] Smith, I. K., Stosic, N., and Kovacevic, A., An improved system for power recovery from higher enthalpy liquid dominated fields, *Proceedings World Geothermal Congress*, London, 1-5, 2005.
[10] Brümmer, A. and Hütker, J., Influence of geometric parameters on inlet losses during the filling process of screw-type motors, *Developments in Mechanical Engineering*, 4, 2009, 105–121.

[11] Hutker, J. and Brummer, A., Thermodynamic Design of Screw Motors for Constant Waste Heat Flow at Medium Temperature Level, *International Compressor Engineering Conference*, London, 1478, 2012.
[12] Kovacevic, A. and Rane, S., 3D CFD Analysis of a Twin Screw Expander, *8th International Conference on Compressors and their Systems*, Woodhead Publishing Limited, 417-429, 2013.
[13] Papes, I., Degroote, J., and Vierendeels, J., New insights in twin screw expander performance for small scale ORC systems from 3D CFD analysis, *Applied Thermal Engineering*, 91, 2015, 535–546.
[14] Papes, I., Degroote, J., and Vierendeels, J., Development of a thermodynamic low order model for a twin screw expander with emphasis on pulsations in the inlet pipe, *Applied Thermal Engineering*, 103, 2016, 909–919.
[15] Andres, R. J. H.,CFD Simulation of a Twin Screw Expander including Leakage Flows, *International Compressor Engineering Conference*, Purdue, 2497, 2016.
[16] Yildiz, A. R. and Ozturk, F., *Hybrid taguchi-harmony search approach for shape optimization*, In: Geem Z (ed) Recent advances in Harmony search algorithm, Springer, Berlin, 89-98, 2010
[17] Yildiz, A. R., Comparison of evolutionary-based optimization algorithms for structural design optimization, *Engineering Applications of Artificial Intelligence*, 26(1), 2013, 327–333.
[18] Abolhasani, H., Moghimi, M., and Ebrahimi, M., Exergetic optimization of twin screw expanders, *International Journal of Exergy*, 30(4), 2019, 360-375.
[19] Kiani, M. and Yildiz, A. R., A Comparative Study of Non-traditional Methods for Vehicle Crashworthiness and NVH Optimization, *Archives of Computational Methods in Engineering*, 23(4), 2016, 723–734.
[20] Pholdee, N., Bureerat, S., and Yildiz, A. R., Hybrid real-code population-based incremental learning and differential evolution for many-objective optimization of an automotive floor-frame, *International Journal of Vehicle Design*, 73(1), 2017, 20–53.
[21] Karagöz, S. and Yildiz, A. R., A comparison of recent metaheuristic algorithms for crashworthiness optimisation of vehicle thin-walled tubes considering sheet metal forming effects, *International Journal of Vehicle Design*, 73(1), 2017, 179–188.
[22] Yildiz, B. S. and Yildiz, A. R., Moth-flame optimization algorithm to determine optimal machining parameters in manufacturing processes, *Materials Testing*, 59(5), 2017, 425–429.
[23] Gopakumar, A. M., Balachandran, P. V., Xue, D., Gubernatis, J. E., and Lookman, T., Multi-objective Optimization for Materials Discovery via Adaptive Design, *Scientific Reports*, 8(1), 2018, 3738.
[24] Kaya, M. and Hajimirza, S., Rapid Optimization of External Quantum Efficiency of Thin Film Solar Cells Using Surrogate Modeling of Absorptivity, *Scientific Reports*, 8(1), 2018, 8170.
[25] Hamza, F., Abderazek, H., Lakhdar, S., Ferhat, D., and Yildiz, A. R., Optimum design of cam-roller follower mechanism using a new evolutionary algorithm, *International Journal of Advanced Manufacturing Technology*, 99(5–8), 2018, 1267–1282.
[26] Yildiz, B. S. and Yildiz, A. R., Comparison of grey Wolf, whale, water cycle, ant lion and sine-cosine algorithms for the optimization of a vehicle engine connecting rod, *Materials Testing*, 60(3), 2018, 311–315.
[27] Noack, M. M., Yager, K. G., Fukuto, M., Doerk, G. S., Li, R., and Sethian, J. A., A Kriging-Based Approach to Autonomous Experimentation with Applications to X-Ray Scattering, *Scientific Reports*, 9(1), 2019, 11809.
[28] Nyshadham, C., Rupp, M., Bekker, B., Shapeev, A. V., Mueller, T., Rosenbrock, C. W., Csanyi, G., Wingate, D. W., and Hart, G. L. W., Machine-learned multi-system surrogate models for materials prediction, *npj Computational Materials*, 5(1), 2019, 51.
[29] Awad, N. H., Ali, M. Z., Mallipeddi, R., and Suganthan, P. N. An improved differential evolution algorithm using efficient adapted surrogate model for numerical optimization, *Information Sciences*, 451, 2018, 326-347.
[30] Yildiz, A. R., A novel hybrid whale–Nelder–Mead algorithm for optimization of design and manufacturing problems, *International Journal of Advanced Manufacturing Technology*, 105(12), 2019, 5091–5104.
[31] Yildiz, A. R., Abderazek, H., and Mirjalili, S., A Comparative Study of Recent Non-traditional Methods for Mechanical Design Optimization, *Archives of Computational Methods in Engineering*, 27, 2019, 1031–1048.
[32] Yildiz, B. S. and Yildiz, A. R., The Harris hawks optimization algorithm, salp swarm algorithm, grasshopper optimization algorithm and dragonfly algorithm for structural design optimization of vehicle components, *Materials Testing*, 61(8), 2019, 744–748.
[33] Yildiz, A. R., Yildiz, B. S., Sait, S. M., Bureerat, S., and Pholdee, N., A new hybrid Harris hawks-Nelder-Mead optimization algorithm for solving design and manufacturing problems, *Materials Testing*, 61(8), 2019, 735–743.
[34] Moctezuma, L. A. and Molinas, M., Multi-objective optimization for EEG channel selection and accurate intruder detection in an EEG-based subject identification system, *Scientific Reports*, 10(1), 2020, 5850.
[35] Abolhasani, H., Moghimi, M., and Ebrahimi, M., Power Recovery in a Gas Pressure Reduction Station using 3D CFD Modeling of a Twin Screw Expander, *Journal of Applied Fluid Mechanics*, 13(4), 2020,1179-1191.
[36] Kurtuluş, E., Yildiz, A. R., Sait, S. M., and Bureerat, S., A novel hybrid Harris hawks-simulated annealing algorithm and RBF-based metamodel for design optimization of highway guardrails, *Materials Testing*, 62(3), 2020, 251–260.
[37] Champasak, P., Panagant, N., Pholdee, N., Bureerat, S., and Yildiz, A. R., Self-adaptive many-objective meta-heuristic based on decomposition for many-objective conceptual design of a fixed wing unmanned aerial vehicle, *Aerospace Science and Technology*, 100, 2020, 105783.
[38] Abderazek, H., Yildiz, A. R., and Mirjalili, S., Comparison of recent optimization algorithms for design optimization of a cam-follower mechanism, *Knowledge-Based Systems*, 2020, 105, 105237.
[39] Forrester, A. I. J. and Keane, A. J., Recent advances in surrogate-based optimization, *Progress in Aerospace Sciences*, 45(1–3), 2009, 50–79.
[40] Zhu, G. J., Guo, P. C., Luo, X. Q., and Feng, J. J., The multi-objective optimization of the horizontal-axis marine current turbine based on NSGA-II algorithm, *IOP Conference Series: Earth and Environmental Science*, 15(4), 2012, 42039.
[41] Bellary, S. A. I., Husain, A., and Samad, A., Effectiveness of meta-models for multi-objective optimization of centrifugal impeller, *Journal of Mechanical Science and Technology*, 28(12), 2014, 4947–4957.
[42] Bellary, S. A. I., Samad, A., Couckuyt, I., and Dhaene, T., A comparative study of kriging variants for the optimization of a turbomachinery system, *Engineering with Computers*, 32(1), 2016, 49–59.
[43] Tosin, S., Friedrichs, J., Sperling, J., and Kozulović, D., Aerodynamic optimization of turboprop turbine blades using a response surface methodology based algorithm, *ASME 12th International Conference on Nano channels, Microchannel, and Mini channels*, American Society of Mechanical Engineers, V01AT02A009-V01AT02A009, 2014.
[44] Gaiser, K., Erickson, P., Stroeve, P., and Delplanque, J.P., An experimental investigation of design parameters for pico-hydro Turgo turbines using a response surface methodology, *Renewable Energy*, 85, 2016, 406–418 .
[45] Badhurshah, R. and Samad, A., Multiple surrogate based optimization of a bidirectional impulse turbine for wave energy conversion, *Renewable Energy*, 74, 2014, 749–760.
[46] Tang, Y., *Computer Aided Design of Twin Screw Compressors*, Ph. D. Thesis, 1995.
[47] Zhao, Q., Chen, Z. H., Huang, Z. G., Zhang, H. H., and Ma, J., Optimization of the aerodynamic configuration of a tubular projectile based on blind kriging, *Scientia Iranica*, 26(1B), 2019, 311–322.
[48] Sóbester, A., Forrester, A. I. J., Toal, D. J. J., Tresidder, E., and Tucker, S., Engineering design applications of surrogate-assisted optimization techniques, *Optimization and Engineering*, 15(1), 2014, 243–265 .
[49] Jakobsson, S., Patriksson, M., Rudholm, J., and Wojciechowski, A., A method for simulation based optimization using radial basis functions, *Optimization and Engineering*, 11(4), 2010, 501–532.
[50] Forrester, A. I. J., Sbester, A., and Keane, A. J., *Engineering Design via Surrogate Modelling*, John Wiley and Sons Ltd, 2008.
[51] Mengistu, T. and Ghaly, W., Aerodynamic optimization of turbomachinery blades using evolutionary methods and ANN-based surrogate models, *Optimization and Engineering*, 9(3), 2008, 239–255.
[52] Kovacevic, A., *Three-Dimensional Numerical Analysis for Flow Prediction in Positive Displacement Screw Machines*, Ph.D. Thesis, School of Engineering and Mathematical Sciences, City University of London, 2002.

ORCID iD

Hormoz Abolhasani https://orcid.org/0000-0001-6677-6889

Mahdi Moghimi https://orcid.org/0000-0002-5450-3338
Mahmoud Ebrahimi https://orcid.org/0000-0002-2288-827X

How to cite this article: Abolhasani H., Moghimi M., Ebrahimi M. Twin Screw Expanders Profile Optimization Using Surrogate-Based Modelling, *J. Appl. Comput. Mech.*, 8(4), 2022, 1141–1153. https://doi.org/10.22055/JACM.2020.33054.2138